Improved math xmlns="http://www.w3.org/1998/Math/MathML">mmultiscripts>mi>Mo/mi>mprescripts>/mprescripts>none>/none>mn>95/mn>/mmultiscripts>/math> neutron resonance parameters and astrophysical reaction rates

P. E. Koehler

Phys. Rev. C **105**, 054306 — Published 12 May 2022

DOI: 10.1103/PhysRevC.105.054306

Improved ^{95}Mo neutron resonance parameters and astrophysical reaction rates

P. E. Koehler[1]

[1] *Los Alamos National Laboratory, Los Alamos, New Mexico 87545, USA*

(Dated: April 26, 2022)

Background: Improved ^{95}Mo neutron resonance parameters and reaction rates are important for nuclear astrophysics, testing nuclear models, and nuclear criticality safety. However, despite many previous neutron capture and total cross section measurements on this nuclide, there still is much room for improvement as well as several discrepancies. For example, there are very few firm resonance spin and parity assignments, average resonance parameters are available only for each parity, the currently recommended astrophysical reaction rate results in disagreements between stellar models and meteoric isotopic anomalies, and there are substantial disagreements in the neutron capture cross section at low energies important for nuclear criticality safety.

Purpose: To obtain an improved set of neutron resonance parameters and astrophysical reaction rates for ^{95}Mo.

Method: High resolution neutron capture and transmission data were measured at the Oak Ridge Electron Linear Accelerator (ORELA) using highly isotopically enriched ^{95}Mo samples. The neutron capture apparatus, data reduction, and analysis were improved so that information contained in the γ-ray cascade following neutron capture were used to assign resonance J^π values. Following this, simultaneous analysis of the new neutron capture and transmission data was used to obtain resonance energies, gamma widths, and neutron widths and their uncertainties to a maximum energy of 10 keV. Accurate neutron capture cross sections also were obtained for the unresolved resonance region to a maximum energy of 500 keV and, together with the new resonance parameters, used to calculate the astrophysical reaction rates in the temperature range from 5 to 30 keV.

Results: A vastly improved set of ^{95}Mo neutron resonance parameters and an astrophysical reaction rate accurate to about 3% were obtained. Firm J^π assignments were determined for 261 of the 314 observed resonances. This is a very large improvement over the previously published 32 firm J^π assignments for 108 resonances. Also, the number of resonances having both firm J^π assignments and Γ_γ values was increased by almost a factor of 24; from 11 to 261. Neutron- and total-radiation-width distributions and average resonance spacings, average total radiation widths, and neutron strength functions were obtained for the six different *s*- and *p*-wave possibilities. Parameters for the lowest *s*-wave resonance, which is most important for criticality benchmarks, were obtained with high accuracy.

Conclusions: Simple modification of the neutron capture apparatus and expansion and improvement of data analysis techniques led to a large increase in firm J^π assignments for ^{95}Mo neutron resonances. The resulting astrophysical reaction rate is 20 - 30% larger than the currently recommended rate at *s*-process temperatures, which should lead to better agreement between stellar models and meteoric isotopic anomalies. The neutron capture cross section at low energies is substantially larger than recommended in the latest evaluation, which is problematical for criticality benchmarks. The average resonance spacing as a function of spin and parity is significantly different from current models. The total radiation-width distributions are significantly broader than predicted by theory and show significant departures from the expected Gaussian shapes.

PACS numbers: 24.30.Gd, 24.60.Dr, 24.60.Lz, 25.40.Lw

I. INTRODUCTION

Improved ^{95}Mo neutron resonance parameters and astrophysical reaction rates are needed for a variety of applications. For example, isotopic abundances of molybdenum isotopes predicted to result from the slow-neutron-capture process (*s* process) in asymptotic giant branch (AGB) stars are particularly sensitive to the ^{95}Mo(n,γ) rate. Failure to obtain satisfactory agreement between molybdenum isotopic abundances predicted by AGB models with that measured in single presolar grains led to the prediction [1] that the currently accepted ^{95}Mo(n,γ) rate [2–4] was 30 percent too low. Improved ^{95}Mo neutron resonance parameters should lead to an improved ^{95}Mo(n,γ) rate, especially at the low temperatures where most of the neutron exposure is predicted to occur in AGB stars.

Neutron resonance parameters also have a long history of being used to test and improve nuclear models. The most stringent tests (e.g. Refs. [5–12]) require large numbers of resonances having firm J^π assignments. Total-radiation-width (Γ_γ) distributions from the new set of resonance parameters described herein have already been used [12] to reveal a problem with nuclear theory that remains unexplained [13]. In addition, average neutron resonance parameters are important for a number of applications such as calibrating nuclear level density and photon strength function shapes [14, 15].

For nuclear criticality safety applications [16], interest in improved resonance parameters for this nuclide stems from the fact that ^{95}Mo is a stable fission product and the primary neutron absorbing isotope in natural molybdenum. For example, molybdenum is encountered in irradiated fuel or in alloys in research and space reactors. The current primary interest to nuclear criticality safety [17] is for fission product credit for transport cases, irradi-

TABLE I. Previous ^{95}Mo+n resonance-parameter measurements. See text for details.

N_{res}	Energy range (eV)	Meas. type	Sample	Ref.
4	45 - 700	T	N and E	[27]
4	45 - 215	C	N	[28]
16	45 - 1145	C	N	[29]
15	45 - 1145	C	N	[30]
13	118 - 1419	T	N	[31]
22	45 - 1420	T	E	[32]
2	44 - 160	T and C	N	[33]
38	110 - 2141	C	E	[22]
51	3130 - 4960	C	E	[25]
57	45 - 2141	C	E	[34]
4	45 - 159	T	N	[35]
47	45 - 1960	T and C	N	[36]
180	5000 - 20000	T	E	[37]

ated fuel storage, and reprocessing plants. The neutron-capture resonance integral, which is dominated by the first resonance near 45 eV, is the most important parameter for nuclear criticality safety applications. The total radiation width and hence the capture kernel for this resonance was reduced in the latest evaluation [18] to yield better performance in criticality benchmarks [19]. However, the evaluated parameters for this resonance are inconsistent with most previously published data and hence new data were requested [16].

Previous measurements from which ^{95}Mo neutron resonance parameters were obtained are summarized in Table I. All of these efforts were hampered by the facts that either only capture (C) or transmission (T) data were obtained and analyzed and/or samples of natural (N) rather than enriched (E) abundance were used. Some also suffered from relatively poor time-of-flight (neutron energy) resolution. A few employed techniques to determine resonance spin and/or parity, although there are relatively few firm J^π assignments. Using the wrong resonance J^π value can result in systematic errors in the extracted neutron and gamma widths. A substantial fraction of resonance parameters in compilations [20, 21] appear to be derived from unpublished [22] data.

In addition, there are no previous published ^{95}Mo neutron resonance data for energies between 2141 and 3130 eV, nor above 4960 eV. In addition to these measurements at resonance energies, data at thermal energy shed light on the spin of resonance(s) dominating the thermal capture [23] and (n, α) [24] cross sections. In addition, data in the unresolved resonance region [25, 26] has been used to extract some average resonance parameters.

In the present work, both neutron capture and transmission were measured using highly enriched samples with high neutron energy resolution, and fitted simultaneously using R-matrix formalism. In addition, a previous technique [30] for determining resonance spins was adopted and improved to determine many more resonance J^π values. Also, the capture measurements were run much longer than usual, resulting in enhanced precision to much higher energies and ultimately much improved resonance parameters across a wider energy range ($0.01 < E_n < 10$ keV).

To obtain a reliable ^{95}Mo(n,γ) rate at s-process temperature requires cross sections to several hundred keV. Therefore, average neutron capture cross sections from 3 to 500 keV, corrected for self shielding, multiple scattering, and the small contributions from other isotopes also were calculated from the data and are reported in this work.

In addition for each of the six possible J^π combinations for s- and p-wave resonances, average resonance spacings ($D_{l,J}$) and neutron strength functions ($S_{l,J}$), corrected for missed small resonances, as well as average total radiation widths ($\langle\Gamma_{\gamma l,J}\rangle$), were extracted from the data and compared to the limited previous data and theory. Finally, $\Gamma_{\gamma l,J}$ and reduced-neutron-width ($\Gamma_n^{l,J}$) distributions for each J^π were extracted from the new resonance parameters and compared to theory.

The experiments and data reduction are described in Section II. Resonance analysis of the data is described in Section III, which is longer than typical so that the new techniques for assigning resonance J^π values can be described in sufficient detail. There are several facilities employing the same type of γ-ray detectors as used in this work, that could benefit from upgrading their systems. This is followed by Section IV in which the procedures used to extract average resonance parameters as well as the results are described. Average cross sections in the unresolved region and resulting astrophysical reaction rates are described in Section V. The new results are compared to previous results in Section VI. Discussion of the impact of the new results on applications and theory can be found in Section VII, followed by conclusions in Section VIII.

II. EXPERIMENT AND DATA REDUCTION

The experimental apparatus has been described previously many times (e.g., see Ref [12, 38] and references contained therein), so only the salient features will be mentioned herein. The Oak Ridge Electron Linear Accelerator (ORELA) [39–41] was operated at a pulse rate of 525 Hz, a pulse width of 8 ns, and a power of 7-8 kW. Neutron energy was determined by time of flight. The samples were metallic molybdenum, enriched to 96.47% in ^{95}Mo. Atom percentages for Mo isotopes present in the sample are given in Table II. Capture and transmission samples were 0.004591 and 0.02507 at/b thick, respectively.

Neutron capture measurements were made at a source-to-sample distance of 38.42 m using a pair of C_6D_6 detectors, and employed the pulse-height-weighting technique. A ^{10}B filter was used to remove overlap neutrons from preceding beam bursts, and a Pb filter was used to reduce γ-flash effects. These filters were placed in the beam at a distance of 5 m from the neutron source. Cross

TABLE II. Atom percentages for Mo isotopes present in the samples.

Atomic number	Atom percentage
94	0.63
95	96.47
96	1.45
97	0.46
98	0.63
100	0.15

section normalization was made via the saturated resonance technique [42] using the 4.9-eV resonance in the ^{197}Au(n,γ) reaction.

A thin ^{6}Li-loaded glass scintillator located 43 cm ahead of the sample in the neutron beam, was used to measure the energy dependence of the neutron flux. Separate sample-out background measurements were made.

Total neutron cross sections were measured via transmission using a ^{6}Li-loaded glass scintillator at a source-to-detector distance of 79.83 m [43]. The measurements were made at the same time, and hence under the same ORELA operating conditions, as the (n,γ) experiments. A ^{10}B filter was used to remove overlap neutrons from preceding beam bursts, and a Pb filter was used to reduce γ-flash effects. These filters were placed in the beam at a distance of 5 m from the neutron source. A separate run was made at a pulse rate of 130 Hz to determine the residual background due to overlap neutrons from preceding beam bursts. This run was made at the same time as the ^{197}Au(n,γ) calibration measurements. The ^{95}Mo sample was exchanged periodically with an empty sample holder, and with polyethylene and bismuth absorbers, which were used for determination of backgrounds.

A relatively minor yet significant change was made to the neutron-capture data acquisition system (DAQ) to allow much improved resonance spin and parity assignments, as described in the next section. The DAQ hardware was rewired so that coincidences between the two C_6D_6 detectors could be recorded and the data replay routine modified to generate pulse-height (PH) versus time-of-flight (TOF) histograms for these data.

III. RESONANCE ANALYSIS

Each resonance is characterized by its energy (E_n), spin and parity (J^π), neutron width ($g_J\Gamma_n$), total radiation width (Γ_γ), and alpha width (Γ_α). Here

$$g_J = (2J+1)\,/\,((2I+1)\,(2j+1))$$

is the spin statistical factor for resonance spin J, neutron spin j, and target spin I. These parameters typically are determined in an R-matrix analysis of the data. However, except for the strongest resonances, determining J^π values via R-matrix analysis is problematic. Assigning J^π values is especially difficult for nuclides such as ^{95}Mo which have non-zero I (and hence more possible J values) and are near the peak of the p-wave neutron strength function (and hence observable neutron widths for the two parities span nearly the same range). In such cases, auxiliary techniques for determining J^π values can be extremely useful. In Subsection III A, an improved version of a technique based on information contained in the γ-ray cascade following neutron capture is described. Following this, in Subsection III B, the R-matrix analysis used to determine the remaining resonance parameters is described. The end result is parameters for many more neutron resonances in ^{95}Mo, and many more firm J^π assignments than previously available.

A. Spin and parity assignments

If the neutron width for a resonance is large enough, then it is well known that its parity can be identified by its shape. For example, the broadest s-wave (p-wave) resonances typically have a characteristic asymmetric (symmetric) shape in transmission. For smaller neutron widths, it becomes impossible to discern resonance parity by transmission shape. However, if $g_J\Gamma_n$ is not too small, it often is still possible to assign resonance parity using both the transmission and capture TOF data. In these cases, if the wrong parity is used in the R-matrix fit, it will not be possible to obtain simultaneous agreement between the fitted and data peak positions in the capture and transmission spectra. These parity-by-shape resonances form the initial calibration set for further J^π assignments.

The next step in assigning resonance spins and parities is an extension of the technique pioneered in Ref. [30]. The basis of the technique is the fact that γ-ray cascades from the capturing state to the ground state are dominated by (mainly electric) dipole transitions. Thus, it is expected that resonances with higher spin will have, on average, higher multiplicity (larger number of γ rays in the cascade from the capturing state to the ground state) as well as lower average energy for the individual γ rays in the cascade. In addition, parity assignment is aided by the fact that almost all low-excitation levels in ^{96}Mo have positive parity and E1 transitions (which change parity) are much stronger than M1 (which leave parity unchanged). Therefore, it is expected that, on average, negative parity resonance will have a larger proportion of high energy transitions to states near the ground state (and hence harder PH spectra) than positive parity ones.

For these reasons, as the PH threshold is raised, the counting rate for higher-spin resonances is attenuated more quickly than for lower-spin ones. At the same time, if two γ-ray detectors are used, the coincidence rate between them is expected to be relatively larger for higher-spin resonances. The power of these two effects for determining resonance spins can be combined by calculating a ratio of coincidence counts (with a relatively low threshold to record as many coincidences as possible) to singles counts with a high threshold. This spin index is systematically larger for resonances having higher spin.

This technique was extended, resulting in more firm spin and parity assignments, in the following ways. First, the data were acquired in event mode so that optimum thresholds could be found during data replay. Second, both upper and lower thresholds were used on the resonance PH spectra. Third, instead of a single ratio of singles to coincidences, all three possible ratios; singles/singles, coincidences/coincidences, and singles/coincidences were used. A program was written to find the optimum PH ranges for separating resonances of different spin and parity, using a boot-strap approach.

To separate resonance spins, three spin indexes were defined for each resonances as ratios of counts in one PH range to counts in a second PH range. For singles/singles and coincidences/coincidences, the two PH ranges were not allowed to overlap.

The technique will be illustrated for the original singles/coincidences ratio used in Ref. [30] for the simplest case where the resonances fall into two spin groups $l = 1$ or 2. There is an initial set of calibration resonance known to belong to one spin group or the other. A spin index is calculated,

$$I_{il} = C_{il}/S_{il}$$

for each resonance i in each group l, where

$$S_{il} = \sum_{k=a}^{b} PH_{kl}$$

is the sum over the singles PH spectrum of resonance i of sping group l over the range from channels a to b, and C_{il} is the sum over the coincidence PH spectrum for the same resonance (over an independent and possibly overlapping PH range c to d). To separate the two spin groups, the program looped through all possible pairs of PH gates to find the pair maximizing quantity

$$D = \left(\overline{I}_1 - \overline{I}_2\right)/\sqrt{r_1 + r_2}$$

where $\overline{I}_1$ and $\overline{I}_2$ are the average spin indexes for each of the two groups and r_1 and r_2 are the mean square differences for each group, for example

$$r_1 = \sum_{i=1}^{N_1} \left(\overline{I}_1 - I_{i1}\right)^2 / (N_1 - 1)$$

where N_1 is the number of calibration resonances in the first spin group. Once this pair of PH gates is found, spin indexes for resonances outside the initial calibration set are calculated and additional resonances belonging to each group are identified and added to each group and the process repeated until the number of resonances identified as belonging to each group stabilizes.

To determine if any resonance j that was not in the calibration sets will be included in either calibration set for the next iteration, the spin index I_j plus or minus its uncertainty

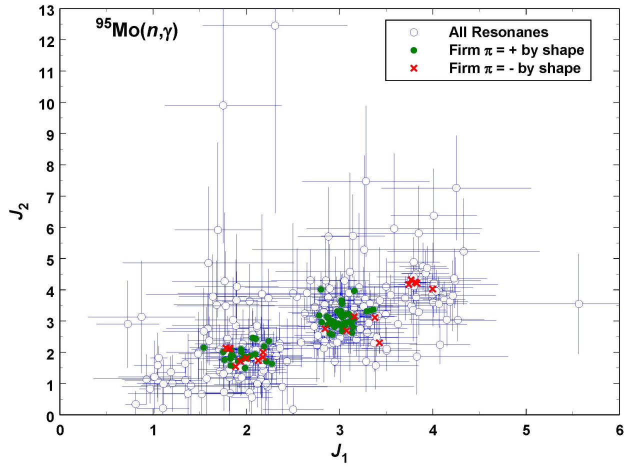

FIG. 1. Singles/singles ratios (J_1) versus coincidences/coincidences (J_2) for all observed resonances (open blue circles with one-standard-deviation error bars), firm positive parity resonances (solid green circles), and firm negative parity resonances (red X's) for PH gates optimizing the separation of (previous firmly assigned) spin 2 and 3 resonances. A linear transformation was applied to the J values in this figure as well as Figs. 2 and 3 so that the groups are centered at integer values between 1 and 4. See text for further details.

$$\sigma_{I_j} = I_j \sqrt{\left(\frac{\sigma_{C_j}}{C_j}\right)^2 + \left(\frac{\sigma_{S_j}}{S_j}\right)^2}$$

(where the $\sigma's$ denote one-standard-deviation statistical uncertainties), for each resonance is compared to the boundary between the two calibration sets. For example, in the case described below where $J^\pi = 2^+$ and $3^+$are being separated, a linear transformation is calculated so that $\overline{I}_1 = 2$ and $\overline{I}_2 = 3$. Then, if (the transformed) $I_j - \sigma_{I_j} > 2.5$ this resonance is assigned to the $J^\pi = 3^+$ group, etc.

The above illustration is for the simplified case where only the single spin index of Ref. [30] is used. Because three spin indexes were used, the criteria used to assign resonances outside the initial calibration sets to either calibration set for the next iteration is more complicated; all three spin indexes for the resonance must be consistent (within the one-standard-deviation uncertainties) with belonging to one or the other calibration set.

The initial set of calibration resonances were those identified as $J^\pi = 2^+$ or 3^+ from previous experiments [30, 34]. The initial set of resonances used to identify additional 2^+ and 3^+ resonances were those identified by their shape as being positive parity. The final set of PH gates resulting from this exercise was then applied to the subset of resonances identified as being negative parity by their shape. These gates separated this resonance set into three groups, two of which roughly overlapped with

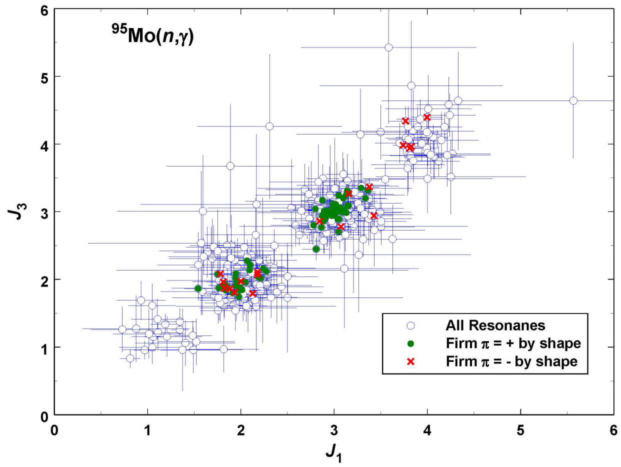

FIG. 2. Singles/singles ratios (J_1) versus singles/coincidences (J_3) for all observed resonances (open blue circles with one-standard-deviation error bars), firm positive parity resonances (solid green circles), and firm negative parity resonances (red X's) for PH gates optimizing the separation of (previous firmly assigned) spin 2 and 3 resonances.

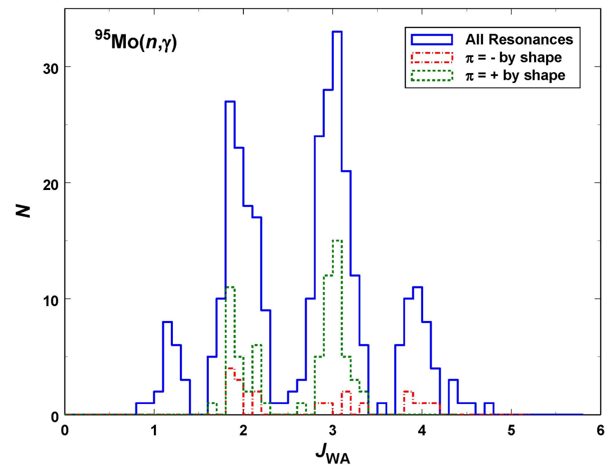

FIG. 3. Weighted averages of the three spin indexes are shown as histograms for all resonances (solid blue), firm positive parity resonances (dashed green), and firm negative parity resonances (dot-dashed red).

the 2^+ and 3^+groups (2^- and 3^-)and a third having larger average spin index (4^-). In practice there should be four p-wave spin groups, but there are fewer 1^- resonances and they are much harder to identify by shape due to their smaller spin statistical factor, $g_J = \frac{1}{4}$, $\frac{5}{12}$, $\frac{7}{12}$, and $\frac{3}{4}$ for $J = 1$, 2, 3, and 4, respectively.

Because there was a small offset between the $J = 2$ and 3 groups for the two parities, it was decided to take one more step before applying the gates to all resonances. Two groups were formed, one for $J = 2$ and the other for $J = 3$, regardless of parity, and a search for new gates best separating these two groups was undertaken. The resulting gates were then applied to all resonances, the results of which are shown in Figs. 1 and 2. In these figures, J_1, J_2, and J_3 denote singles/singles, coincidences/coincidences, and singles/coincidences ratios, respectively. Also, a linear transformation was applied to these ratios so that the peaks appear at 1, 2, 3, and 4, corresponding to the allowed spins for s- and p-wave resonances in ^{95}Mo.

Fig. 3, in which a histogram of the weighted averages of the three spin indexes for all resonances is shown, provides further illustration of how well resonance spins could be assigned. Four distinct, well separated peaks corresponding to the four possible resonance spins are clearly visible.

The final step was to separate the J =2 and 3 groups into positive and negative parity. The same general procedure was followed, albeit with different sets of initial and calibration resonances. For example, to separate the $J = 2$ group by parity, the initial calibration resonances were those previously identified as having this spin and whose parity had been assigned by shape, as explained above. The same program was then run to identify new positive and negative parity resonances with this spin. The resulting PH gates for optimally separating the two parities were different from the optimum gates for separating spins.

Results of separating the J =2 and 3 groups into the two parities is shown in Fig. 4, where the weighted averages of the three spin indexes are plotted versus the weighted averages of the three parity indexes for J =2 and 3 resonances assigned firm parity. For a resonance to be assigned firm parity (in addition to those assigned by shape, as discussed above), at least one of the parity indexes must be at least one standard deviation from the boundary between parities for this index and none of the other parity indexes is more than one standard deviation on the other side of the boundary.

Because J =1 and 4 resonances are necessarily p wave, resonances with firm J =1 and 4 assignments were also assumed to be firm negative parity. In addition, the five 4^- resonances at 1789, 2298, 2952, 5581, and 5721 could be assigned firm negative parity by shape, as discussed above.

B. *R*-matrix analysis

The spin and parity assignments described in the previous subsection were kept fixed in the subsequent R-matrix analysis and found to result in good agreement with the data. The neutron capture and transmission data were fitted simultaneously using the R-matrix program SAMMY [44]. Channels up to d waves were included, although only s- and p-wave resonances were assigned.

Preliminary fitting had already been done to identify

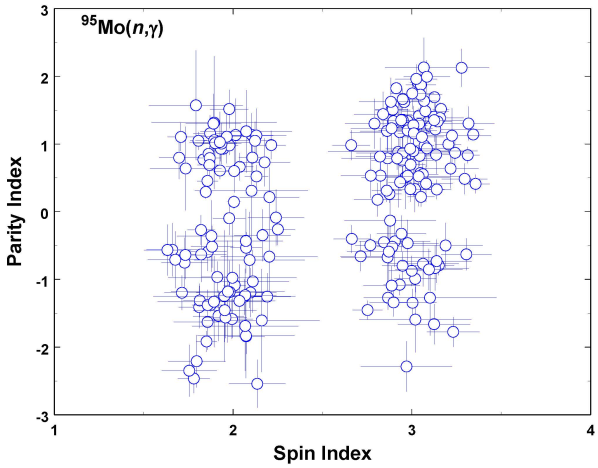

FIG. 4. Weighted averages of the three spin indexes versus weighted averages of the three parity indexes for all spin 2 and 3 resonances assigned firm parity. A linear transformation was applied to the spin index so that the groups are centered at 2 and 3. Similarly, a linear transformation was applied to the parity index so that the groups were centered at -1 and 1. See text for details.

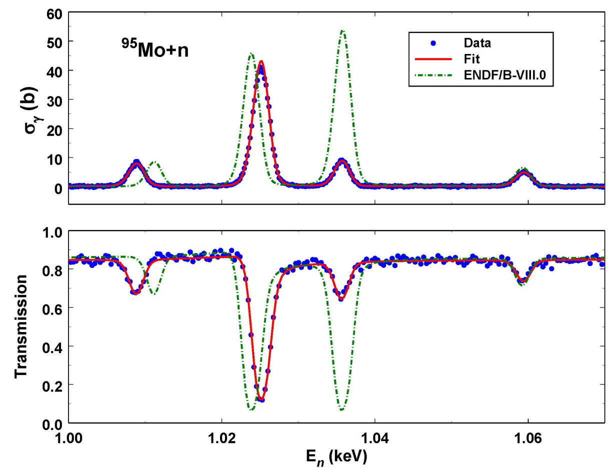

FIG. 5. ^{95}Mo neutron transmissions (bottom) and capture cross sections (top) from 1.0 to 1.07 keV. Data are shown as solid blue circles with one-standard-deviation error bars, SAMMY R-matrix fits as red curves, and ENDF/ B-VIII.0 [18] as dot-dash green curves.

resonances having firm parity by shape, as discussed in the last subsection, and to obtain preliminary energies and widths for all resonances.

The first step was to fit the radii, and widths and energies for resonances having fairly large neutron widths. The s-wave radii affect the transmission level between resonances as well as the shapes of resonances with larger neutron widths. In the present case, it was not possible to obtain good fits to the largest s-wave resonances with a common radius for the two s-wave spins. Therefore, the $J^\pi = 2^+$ and 3^+ radii were allowed to vary independently and the final fitted values were found to be significantly different; 8.21 and 6.81 fm for $J^\pi = 2^+$ and 3^+ resonances, respectively. A single radius of 7.32 fm for p-wave resonances was found to result in acceptable fits to the data.

The next step was to obtain preliminary fits to the smaller resonances. The energies and widths were used to calculate the energy ranges for projecting the PH spectra used to assign spins, as described in the last subsection. For isolated resonances, PH spectra were projected over a width equal to either the natural width (sum of the neutron, gamma, and alpha widths) or the ORELA resolution at the resonance energy, whichever was larger, including Doppler broadening. If the resonance was not totally resolved, the range in either or both the low- and high-energy directions were reduced to discriminate against contributions from nearby resonance.

If the resonance spin assigned as described in the last subsection was different from the preliminary value, the resonance was refitted to obtain final neutron and gamma widths. Resonances also were refitted, even if their spin assignment was unchanged, if refitting a nearby resonance resulted in a degradation of the fit (e.g., due to a change in interference effects).

When the neutron width is small enough, there is little sensitivity to the gamma width in the fitting. This effect depends on energy, but is especially apparent if the resonance is not visible or causes only a very small dip in the transmission data. In the past (e.g. Refs. [45, 46]), gamma widths for these resonances were held fixed at the average gamma width for the given spin and parity. However, in the present case it was found that this sometimes resulted in fits which were not in good agreement with the data. Therefore, both the neutron and gamma widths for all resonances were allowed to vary. To obtain reliable uncertainties for resonances having the smallest neutron widths, the initial gamma-width uncertainty (the SAMMY "fudge factor" [44]) sometimes had to be increased to 0.99, and some gamma-width uncertainties are quite large.

Once the capture and transmission data were well fitted, the final step was to fit the (n, α) data [47], during which only the alpha widths were allowed to vary. This procedure was used because the alpha cross section and widths are so small that they have negligible impact on the fits to the transmission and capture data. Conversely, the fitted alpha widths are sensitive to the other resonance parameters, most importantly the spins and the neutron widths, and the new values for these parameters for some resonances obtained here are different from those used in Ref. [47].

Example fits to the new capture and transmission data are shown in Figs. 5 and 6. The (n, α) data and new SAMMY fits are shown in Fig. 7. The final resonance parameters are given in the supplemental material [48].

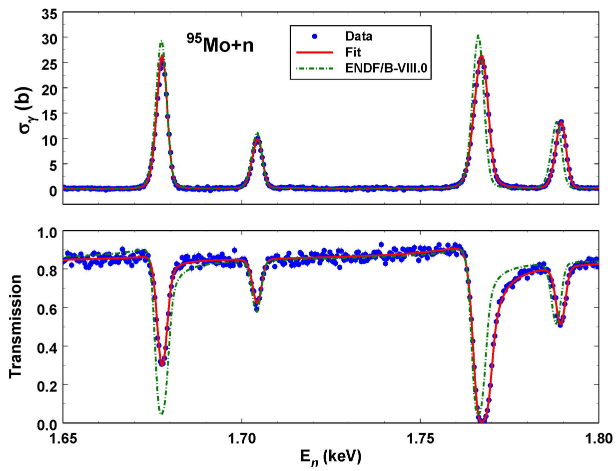

FIG. 6. ^{95}Mo neutron transmissions (bottom) and capture cross sections (top) from 1.65 to 1.80 keV. Data are shown as solid blue circles with one-standard-deviation error bars, SAMMY R-matrix fits as red curves, and ENDF/ B-VIII.0 [18] as dot-dash green curves.

IV. AVERAGE RESONANCE PARAMETERS

Obtaining accurate average resonance spacings and neutron strength functions requires corrections for missed small resonances. The technique of Ref. [49], which is based on the assumption that the reduced neutron widths follow a Porter-Thomas [50] distribution (PTD), was used. A major advantage of this technique, compared to those based on the assumed resonance spacing distribution, is that the resonances which are missed, and hence the threshold required to make the corrections, are readily apparent in the data, as demonstrated in the supplemental material [48].

The resulting corrected average resonance spacings and neutron strength functions, assuming all tentative J^π assignments are correct, are given in Table III. Uncertainties on $D_{l,J}$ and $S_{l,J}$ values in this table were calculated according to Ref. [20]. Plots of the data illustrating the threshold used and the size of the corrections are given in the supplemental material [48].

In principle, uncertainties, especially for the average resonance spacings, will be larger due to the effects of miss-assigned spins and parities. However, it seems likely that miss-assignments will at least partially balance out in this regard. Also, many of the tentative assignments are below the threshold used to correct for missed resonances and so do not affect the corrected average spacings and neutron strength functions. To estimate the maximum effect miss-assignments could have on these average resonance parameters, the correction procedure for missed small resonances was repeated with the same threshold, but using only firm J^π assignments. The resulting $D_{l,J}$ ($S_{l,J}$) values changed to 290 ± 36 (0.238 ± 0.079), 143 ± 11 (1.12 ± 0.23), 208 ± 19 (0.76 ± 0.19), 186 ± 16 (0.68 ± 0.17), 218 ± 18 (0.165 ± 0.037), and 111.8 ± 6.6 (0.311 ± 0.050) for 1^-, 2^-, 3^-, 4^-, 2^+, and 3^+ resonances, respectively. This exercise indicates that the potential impact of miss-assignments on the $S_{l,J}$ values is very small. The potential impact also is relatively small on the $D_{l,J}$ values, except for 3^- resonances, which is not surprising as this J^π value has the largest fraction of tentative assignments.

TABLE III. Average parameters for ^{95}Mo+n resonances. See text for details.

J^π	$\langle\Gamma_{\gamma l,J}\rangle$ (meV)	σ_N (meV)	$10^4 S_{l,J}$	$D_{l,J}$ (eV)
1^-	523^{+60}_{-55}	175^{+56}_{-47}	0.240 ± 0.080	276 ± 34
2^-	308^{+22}_{-21}	129^{+20}_{-17}	1.24 ± 0.24	121.8 ± 8.5
3^-	376^{+23}_{-21}	103^{+18}_{-14}	0.89 ± 0.19	142 ± 11
4^-	278^{+23}_{-22}	113^{+21}_{-17}	0.72 ± 0.17	166 ± 14
2^+	204.5 ± 9.7	$60.4^{+7.5}_{-6.5}$	0.171 ± 0.035	184 ± 14
3^+	214.5 ± 9.0	$72.9^{+7.6}_{-6.8}$	0.318 ± 0.049	103.3 ± 5.9

According to Ref. [50], Γ_γ values for a given J^π are expected to follow a χ^2 distributions with many degrees of freedom, $\nu_\gamma \approx 100$. For such large values of ν_γ, a χ^2 distribution is very close to Gaussian in shape. One advantage of using a Gaussian rather than χ^2 distribution for the analysis is that uncertainties $\Delta\Gamma_\gamma$ can easily be included. Therefore, the technique of Ref. [51] was used to estimate most likely values for the means $\langle\Gamma_\gamma\rangle$ and standard deviations σ_N of the Γ_γ distributions for resonances of each J^π. Resulting maximum-likelihood (ML) estimates for these parameters are given in Table III and the corresponding Gaussian distributions are compared to the data in Fig. 8.

V. AVERAGE CROSS SECTIONS AND ASTROPHYSICAL REACTION RATES

Neutron capture cross sections averaged over coarse energy bins are shown in Fig. 9 and listed in Table IV. The relatively small corrections for multiple scattering and resonance self-shielding were calculated using the code SESH [52]. These data also were corrected for isotopic impurities in the sample using previous measurements [25]. The cross sections in Fig. 9 have been multiplied by the square root of the energy at the center of each bin, effectively removing the underlying 1/v component, to facilitate comparison with previous data. Cross sections calculated from the resonance parameters of this work also are shown in this figure. Uncertainties common to both methods of calculating average cross section (e.g., due to normalization) are not included in the table or figure and therefore represent one-standard deviation statistical uncertainties only. The good agreement between average cross sections obtained by the two techniques attests to the accuracy of the background subtraction and corrections applied to the data in this work.

Astrophysical reaction rates calculated following the

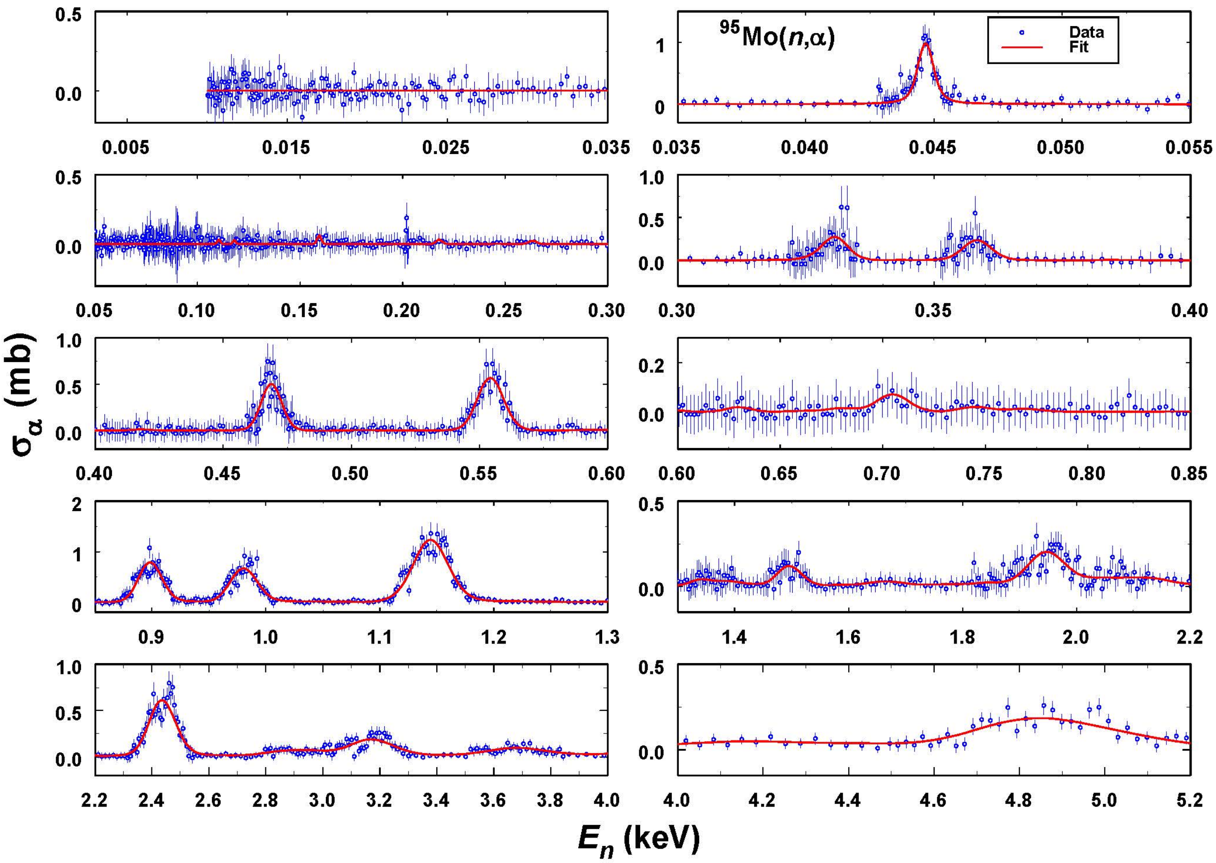

FIG. 7. ^{95}Mo(n,α) cross sections [47] from 10 eV to 5.2 keV (the highest energy fitted in this work for this cross section). Data are shown as open blue circles with one-standard-deviation error bars and SAMMY R-matrix fits as red curves.

TABLE IV. Average $^{95}Mo(n,\gamma)$ cross sections.

Energy (keV)	$\langle\sigma_\gamma\rangle$ (mb)	Energy (keV)	$\langle\sigma_\gamma\rangle$ (mb)
3 - 5	1277.0 ± 2.5	80 - 100	157.78 ± 0.82
5 - 7.5	949.6 ± 2.2	100 - 120	137.9 ± 1.1
7.5 - 10	784.2 ± 2.2	120 - 150	124.79 ± 0.68
10 - 12.5	675.5 ± 2.1	150 - 175	112.39 ± 0.69
12.5 - 15	612.4 ± 2.2	175 - 200	102.14 ± 0.67
15 - 20	505.1 ± 1.5	200 - 225	92.98 ± 0.69
20 - 25	453.6 ± 1.5	225 - 250	87.86 ± 0.65
25 - 30	381.0 ± 1.5	250 - 300	80.51 ± 0.46
30 - 40	320.5 ± 1.1	300 - 350	74.51 ± 0.41
40 - 50	276.5 ± 1.1	350 - 400	69.23 ± 0.45
50 - 60	231.0 ± 1.0	400 - 450	68.16 ± 0.39
60 - 80	190.71 ± 0.74	450 - 500	68.60 ± 0.35

TABLE V. Average $^{95}Mo(n,\gamma)$ reaction rates.

kT (keV)	$\langle\sigma v\rangle/v_T$ (mb)	kT (keV)	$\langle\sigma v\rangle/v_T$ (mb)
5	1018 ± 31	12	620 ± 19
6	923 ± 28	15	541 ± 16
7	848 ± 26	18	491 ± 15
8	786 ± 24	20	451 ± 14
9	735 ± 22	25	390 ± 12
10	691 ± 21	30	346 ± 10

technique of Ref. [55] are listed in Table V. Rates calculated SAMMY agreed to withing 0.5%. Statistical uncertainties are negligible when compared to the overall normalization uncertainty. From the uncertainties in the $^{197}Au(n,\gamma)$ and $^{6}Li(n,\alpha)$ cross sections, the statistical precision of the calibration measurements, the repeatability of the calibration runs, and uncertainties in the sample size and isotopic abundances, on overall uncertainty of 3% - 4% was calculated. These systematic uncertainties apply to both the average cross sections in Table IV and the reaction rates in Table V, but have been applied only to the values in the latter table.

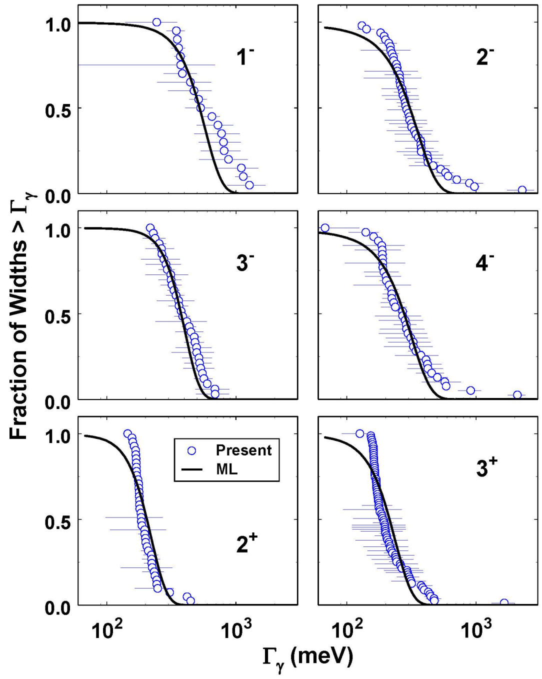

FIG. 8. Cumulative Γ_γ distributions for resonances of each J^π. Data from the present work are shown as open blue circles with one-standard-deviation error bars. Solid curves depict Gaussian distributions resulting from a ML analysis of the data using the method of Ref. [51]. See text for details.

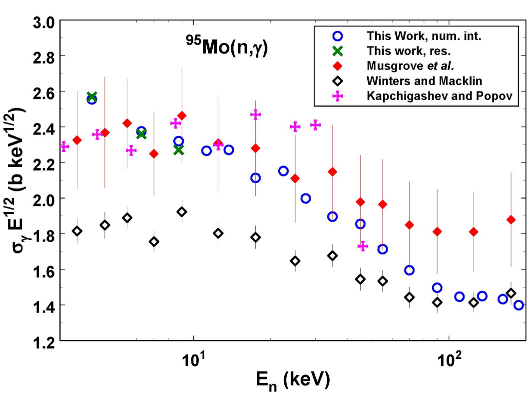

FIG. 9. Reduced $^{95}Mo(n,\gamma)$ cross sections averaged over coarse energy bins. Results from this work are shown as open blue circles (calculated via numerical integration) and green X's (calculated from the resonance parameters). Results from previous work [25, 53, 54] are shown as solid red diamonds, magenta crosses, and open black diamonds respectively. One-standard-deviation statistical uncertainties are smaller than the size of the symbols for this work. Error bars depict statistical (total) uncertainties for Ref. [54] ([25]). No uncertainties were reported for Ref. [53].

VI. COMPARISON TO PREVIOUS WORK

Thermal cross sections and the capture resonance integral calculated from resonance parameters of the present work, the resonance parameters themselves, average resonance parameters, average cross sections, and astrophysical reaction rates are compared to previous work in the following subsections.

A. Comparison to previous thermal cross sections

As discussed in Section VII, the capture cross sections near thermal energy is important from nuclear criticality safety applications, so some care was taken to reproduce the data in this region. A negative energy level, whose parameters are given in the supplemental material [48], was adjusted to yield the reported thermal (n,γ) [56] and (n,α) [24] cross sections. The $J = 3$ spin assignment of this level differs from the $J = 2$ assignment given in compilations [20, 21] for the following reasons.

First, according to Ref. [23], on the basis of two-step cascade measurements, the thermal neutron capture cross section is dominated by $J = 3$. Second, according to Ref. [24], the thermal (n,α) cross section is dominated by the α_0 channel. This implies $J = 2$ because $J = 3$ ^{95}Mo resonances are parity forbidden from α decaying to the 0^+ ground state of ^{92}Zr. However, without the 3^+ negative-energy level, the thermal (n,α) cross section is 53.5 μb, which is nearly twice the measured value. By adjusting the alpha width of the negative energy level it is possible to reduce the thermal (n,α) cross section to the measured value, presumably through destructive interference with 3^+ resonance(s). To check that the thermal (n,α) cross section is predominantly due to 2^+ resonances, the alpha widths of 2^+ resonances up to and including the 1144-eV one were set equal to zero. The resulting thermal (n,α) cross section was reduced to 10.5 μb, in qualitative agreement with Ref. [24].

The capture resonance integral, calculated from the present resonance parameters using Eq. 2.86 in Ref. [20] is $I_\gamma = 114.2$ b. A $1/v$ component calculated from Eq. 2.88 of this same reference, using the thermal cross section of Ref. [56] yields an additional 6.0 b, for a total of $I = 120.2$ b, in agreement with the value of 121$\pm$ 1 b of Ref. [36], but significantly higher than the most recent evaluation [18] value of 104.4 b.

B. Comparison to previous resonance parameters

Of the firm J^π assignments in Refs. [22, 28–30, 34], the only disagreement with the present work is the 418-eV resonance which was assigned negative parity in Ref. [34], but is assigned positive parity in the present work. This is one of the smallest resonances with a firm parity assignment, so perhaps this conflict is not too surprising. Of the 71 resonances in Ref. [37] overlapping with the present work, 32 (27) have J (l) assignments which disagree. The J values in Ref. [37] "were assigned arbitrarily" and there was no description of how l values were assigned. Of the 56 resonances in the most recent evaluation [18], 43 have spins consistent with the present work.

For Γ_γ values there is, in general, agreement to within the uncertainties between this work and Refs. [22, 27, 29, 32, 36]. In contrast, both Refs. [25, 35] are systematically low compared to the present work, and the differences between this work and Ref. [37] are substantially larger than is consistent with the size of the error bars, indicating that uncertainties have been underestimated. As SAMMY was used in both the present work and Ref. [37], perhaps this is an indication that resonance-parameter uncertainties calculated by this code are systematically small.

Total radiation widths from the most recent evaluation [18] appear to have predominantly been assumed to be constant at two different values, depending on the parity of the resonance, and so no comparison to these values are made herein.

With the exception of Refs. [22, 27, 57], the agreement between the current and previous neutron widths is poor. For example, the results of Ref. [36] are systematically low compared to the present work. This systematic trend is even clearer if the 21 resonances in Ref. [36] having incorrect J assignments, according to the present work, are excluded. Note that counterparts to the resonances at 358., 679.3, and 896 eV in Ref. [57] and at 6469 and 7340 eV in Ref. [37] could not be identified in the present work. Conversely, there are 82 resonances in the 5 - 10 keV region observed in the present work that were not reported in Ref. [37].

Neutron widths from the most recent evaluation [18] also are,in general, in poor agreement with this work. In particular, there are several resonances for which the evaluated neutron widths differ from the present work by many times the uncertainties. As can be seen in Figs. 5 and 6, the evaluated widths are clearly in error. In the case of the 1036-eV resonance, it appears to be a simple case of the decimal point being misplaced in the evaluation table.

Although there are additional neutron widths listed in Ref. [25], they are given without uncertainties and were calculated assuming $g = 0.5$ and $\Gamma_\gamma = 150$ meV. Hence, it is more worthwhile for these resonances to compare capture kernels ($g\Gamma_n\Gamma_\gamma/\Gamma$). On average, the capture kernels of Ref. [25] are 9% smaller than the present work. This difference is within the 12% normalization uncertainty given in Ref. [25]. In addition, the scatter is larger than expected for the size of the error bars, indicating that the present and/or previous uncertainties have been underestimated.

TABLE VI. Average s-wave ^{95}Mo+n parameters from previous work. See text for details.

Ref.	$\langle\Gamma_{\gamma 0}\rangle$ (meV)	$10^4 S_0$	D_0 (eV)
[27]	-	0.40 ± 0.14	370 ± 120
[57]	-	0.55 ± 0.40	220 ± 50
[31]	-	0.38 ± 0.15	-
[32]	185 ± 15	$0.5^{+0.5}_{-0.2}$	284 ± 49
[22]	170 ± 15	-	102 ± 10
[25]	-	0.45 ± 0.25	-
[36]	179.4 ± 9.7	0.44 ± 0.14	80 ± 25
[37]	-	0.294 ± 0.058	-
[26]	-	0.4 ± 0.1	-
[18]	150	0.45	69.4
This work	209.9 ± 6.6	0.489 ± 0.060	66.2 ± 3.0

C. Comparison to previous average resonance parameters

Average resonance parameters reported in previous works are shown in Tables VI and VII and can be compared to results from this work shown in Table III. There are a few caveats that should be mentioned about the numbers in Tables VI and VII. First, it is not always clear from previous publications just what the quoted uncertainties represent and some values were given without uncertainties or with uncertainties calculated in a non-standard way. For example, the D_0 values in Ref. [32] is given without uncertainty; the uncertainty given in Table VI was calculated according to Ref. [20]. Also, the S_0 uncertainty given in Ref. [36] and S_1 uncertainty of Ref. [37]) were calculated in a non-standard way which yields a very small value; so again the values given in Table VI were calculated according to Ref. [20]. In addition, the D_0 and $\langle\Gamma_{\gamma 0}\rangle$ values from Ref. [25] were estimated using resonance parameters from previous work and so are not included in Table VI. Also, the neutron strength functions from Refs. [25] and [26] were estimated from fits to their average cross section data, not from resonance parameters as is the case for all the other references listed in Tables III, VI, and VII.

With the exception of $\langle\Gamma_{\gamma 0}\rangle$ values from Ref. [36], none of the previous works reported average resonance parameters for individual J^π values. Therefore, the neutron strength functions, average resonance spacings, and average total radiation widths from the present work given in Tables VI and VII were combined for each parity. In the case of the neutron strength functions, this was just a simple matter of summing the individual values and for the spacings summing the inverses. In the case of average total radiation widths for the present work and Ref. [36], the values given in Tables VI and VII are the weighted averages of the values for each parity.

The standard- or z-score can be used to quantify the level of agreement between two measured values x_1 and x_2 having one-standard-deviation uncertainties σ_1 and σ_2; $z = (x_1 - x_2)/\sqrt{\sigma_1^2 + \sigma_2^2}$. For example, $|z| > 2$ suggests there is less than a 5% chance that the two values

TABLE VII. Average p-wave ^{95}Mo+n parameters from previous work. See text for details.

Ref.	$\langle\Gamma_{\gamma 1}\rangle$ (meV)	$10^4 S_1$	D_1 (eV)
[57]	-	6.4 ± 4.0	-
[32]	227 ± 67	5^{+10}_{-3}	-
[22]	-	10 ± 2.5	51 ± 5
[25]	-	7.5 ± 2.5	-
[26]	-	3.8 ± 0.1	-
[18]	180	6.54	34.7
This work	319 ± 12	3.09 ± 0.35	40.1 ± 1.7

are in agreement.

There is generally poor agreement ($|z| > 2$) between the present and previous work for average total radiation widths and average resonance spacings, except for $\langle\Gamma_{\gamma 0}\rangle$ of Ref. [32], D_0 of Refs. [18, 36], and $\langle\Gamma_{\gamma 1}\rangle$ of Ref. [32]. On the other hand, there is generally good agreement for the neutron strength functions except for S_0 of Ref. [37] and S_1 of Refs. [18, 22]. In particular, there is poor agreement between the present work and the latest evaluation [18] except for S_0 and D_0.

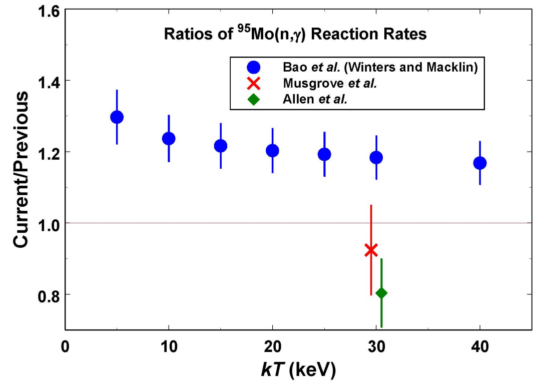

FIG. 10. Ratios of $^{95}Mo(n,\gamma)$ astrophysical reaction rates. Ratios of this work to Refs. [25, 54, 59] are shown as solid blue circles, red X's, and green diamonds, respectively. Error bars depict one-standard-deviation uncertainties. The data points for Refs. [25, 59] have been offset slightly in temperature for clarity.

D. Comparison to previous average capture cross sections and astrophysical reaction rates

Average cross sections from this work are compared to previous measurements in Fig. 9. In general, the data of Refs. [25, 53] agree with the present work whereas the data of Ref. [54] disagree with this work for energies below about 70 keV, by as much 30% at the lower energies.

The average cross sections and astrophysical reaction rates reported in Refs. [25, 54] are actually based on the same data although the reported average cross sections and astrophysical reaction rates differ by about 30%. A small correction (factor of 0.9833) for a programming error [58] to the original data of Ref. [25] was applied in Ref. [54], but the bulk of the difference remains unexplained.

Ratios of astrophysical reaction rates from this work to previous work are shown in Fig. 10. The data of this work agree with those of Refs. [25, 59] ($z = 0.54$ and $z = 1.6$, respectively) but are significantly larger than those of Ref. [54] ($z > 3.5$).

VII. DISCUSSION

Impacts of the new data of this work on nuclear astrophysics, nuclear models, and nuclear criticality safety are described in this section.

Astrophysical rates from this work are 20 - 30% larger than the currently recommended rate [2–4], which is based on the work of Ref. [54], which is a reanalysis of the data of Ref. [25] that resulted in a 30% reduction in the rate for unspecified reasons. The rate from this work is very close to that predicted in Ref. [1] and hence should result in much better agreement between molybdenum isotopic abundances predicted by AGB models of the s process and that measured in single presolar grains. Previous results [45, 60] obtained with the same systems used in this work agree with data [61, 62] from another laboratory using a different detection system, neutron source, and analysis techniques to within the published uncertainties of about 3%. Hence, it seems likely that the rate from this work is more reliable than Ref. [54].

There are several implications of the new resonance parameters of this work for basic nuclear physics. For example, the large fluctuations in the measured Γ_γ distributions are in sharp disagreement with simulations in the framework of the nuclear statistical model [12, 13]. However, average total radiation widths are used to calibrate photon strength functions measured using the Oslo technique (for example see Ref. [15]) and so they are reported in Table III. However, given the disagreement with theory and the fact the distributions shown in Fig. 8 are only approximately Gaussian, the average total radiation widths in Table III should be considered as approximations.

The assumption that reduced neutron widths follow the Porter-Thomas distribution (PTD) [50] can be tested with fairly high precision using the combined 2^+ and 3^+ resonances from this work. The PTD is a χ^2 distribution with one degree of freedom, $\nu = 1$. The ML technique of Ref. [7] was used to estimate the most likely number of degrees of freedom value ν_{ML} from the data. This technique employs an energy-dependent threshold to guard against systematic errors due to missed small resonances

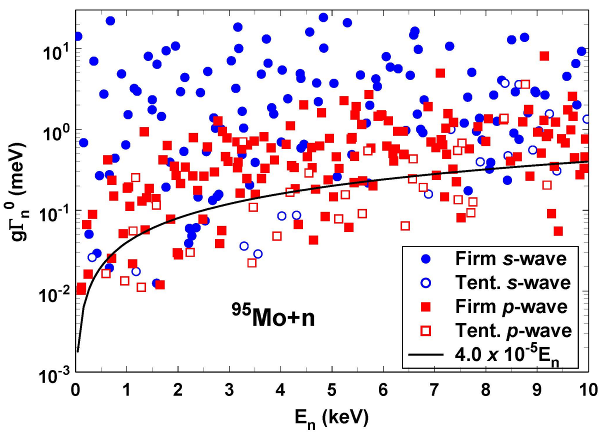

FIG. 11. Reduced neutron widths ($g\Gamma_n^0 = g\Gamma_n/\sqrt{E_n}$) vs. E_n for all resonances fitted in this work. Firm s- and p-wave resonances are shown as solid blue circles and solid red boxes, respectively and tentative s- and p-wave resonances as open blue circles and open red boxes, respectively. An energy-dependent threshold used to guard against systematic errors due to missed small resonances and many of the resonances of uncertain parity is shown as the solid black curve. See text for details.

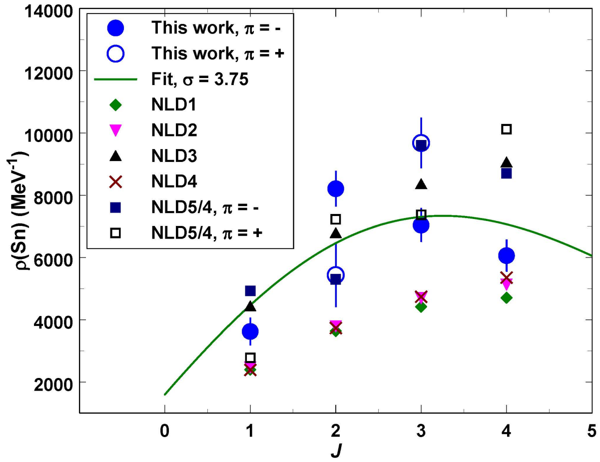

FIG. 12. Nuclear level densities, calculated from the average resonance spacings in Table III, for negative (solid blue circles) and positive (open red circles) parity. The solid green curve depicts a least-squares fit to the data, from which a spin-cutoff parameter of $\sigma = 3.75 \pm 0.94$ was extracted. Also shown are the level densities at Sn predicted by five nuclear-level-density models in Talys1.8. Note that Talys1.8 model 5 level densities have been divided by 4.0. See text for details.

(which tend to lead to systematically large ν_{ML}) and to exclude p-wave resonances (which tend to lead to systematically small ν_{ML}). A typical threshold, together with reduced neutron widths from this work are shown in Fig. 11. The ML analysis was repeated using threshold coefficients between 1.5×10^{-5} to 8.0×10^{-5}, with results agreeing at the 2σ level. For example, the result of the ML analysis with the threshold shown in Fig. 11 is $\nu_{ML} = 0.76 \pm 0.21$, which is consistent with the PTD at the 1.1σ level. Unfortunately, there are still several resonances of uncertain parity above threshold, so there may be sizeable systematic error in this result. By the time the threshold is raised far enough to eliminate all resonances of uncertain parity, there are so few resonances left that the precision is very poor. Hence, despite the large improvement in J^π assignments in this work, this result serves to further illustrate that nuclides near the peak of the p-wave neutron strength function should not be used to test the PTD; It is still too difficult to reliably separate s- from p-wave resonances for these nuclides.

Accurate knowledge of the nuclear J^π distribution as a function of excitation energy is vital for applications using indirect techniques to constrain important neutron reaction cross sections (e.g. Ref. [14]). It recently was demonstrated [63] that the nuclear J distribution as a function of excitation energy in ^{198}Au may be quite different from commonly employed models (e.g. Ref. [64]). With average resonance spacings, and hence nuclear level densities for six J^π values at the neutron separation energy S_n, this work appears to be the first time the nuclear spin distribution at S_n can be adequately constrained by data.

The D_l values from Table III, converted to level densities ρ, are displayed in Fig. 12. Also shown in this figure is a least-squares fit to these data using the common formula in which the spin distribution is parameterized in terms of the spin-cutoff parameter σ, $\rho_J = \frac{2J+1}{2\sigma^2} e^{-\frac{J(J+1)}{2\sigma^2})}\rho$. The fitted value, $\sigma = 3.75 \pm 0.94$, is consistent with the range used in common nuclear level density models, for example those used in the nuclear statistical model TALYS [65] version 1.8 span the range from $\sigma = 4.60$ to 4.99. However, the assumed shape is not in very good agreement with the data, and the data also indicate there is a parity dependence to the level density.

Level densities for the five models in Talys1.8 for which the needed information could be extracted also are shown in Fig. 12. Models 1 - 4 (Constant temperature plus Fermi gas, Back-shifted Fermi gas, generalised superfluid, and microscopic densities from Goriely's tables, respectively) are parity independent and have nearly the same J dependence. Models 1, 2, and 4 are nearly identical, and model 3 is closest to the data. The only model (5, microscopic densities from Hilaire's combinatorial tables) with parity dependence has a dependence opposite to the data; The negative-parity model is in better agreement with the positive-parity data and vice versa.

To resolve the discrepancy between ENDF/B-VII.0 [66] and integral benchmark results [19], Γ_γ for the 44.9-eV resonance was reduced to 120 meV in the ENDF/B-VIII.0 evaluation [18]. It is the capture kernel, $(g\Gamma_n\Gamma_\gamma/(\Gamma_n + \Gamma_\gamma)$, that is most relevant for this

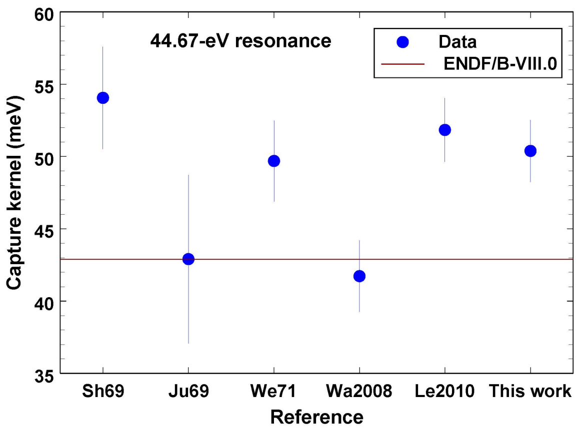

FIG. 13. Capture kernels for the 44.67-eV resonance from this and previous [22, 32, 33, 35, 36] work (solid blue circles with one-standard-deviation error bars) are compared to the most recent evaluated value [18] (solid red line).

application and, as shown if Fig. 13, the ENDF/B-VIII.0 kernel for this resonance is ruled out with high confidence ($z = 3.5 - 5.7$) by four of the six measurements, including this work. Note that for this figure and the quoted z scores, a normalization uncertainty of 3% was added (in quadrature) to the statistical uncertainties on the neutron and gamma widths of this work and Ref. [36]. The only previous measurements in agreement with ENDF/B-VIII.0 are the two most limited with only two [33] and four [35] resonances reported. In addition, the Γ_γ values for the other resonances reported in Refs. [33, 35] also are all systematically smaller than this work. Hence, there can be little doubt that the ENDF/B-VIII.0 evaluated parameters for the 44.9-eV resonance are ruled out by the data and therefore another solution to the integral benchmark discrepancy must be found.

VIII. CONCLUSIONS

Simple modification of the neutron capture apparatus and expansion and improvement of data analysis techniques led to a large increase in firm J^π assignments for ^{95}Mo neutron resonances. This together with simultaneous analysis of new high resolution neutron capture and transmission data resulted in a vastly improved set of neutron resonance parameters for this nuclide. For example, firm J^π assignments were determined for 261 of the 314 observed resonances. This is a very large improvement over the previously published 32 firm J^π assignments for 108 resonances. Also, the number of resonances having both firm J^π assignments and Γ_γ values was increased by almost a factor of 23; from 11 to 261. This has made it possible to extract average resonance spacings, neutron strength functions, average total radiation widths, and total radiation-width distributions for all six s- and p-wave J^π values. These data go far beyond similar data for any nuclide and should be useful for applications such as nuclear astrophysics, nuclear criticality safety, and for testing and improving nuclear models and random matrix theory. Comparison of the present to previous data yields mixed results and indicates a new evaluation is needed.

ACKNOWLEDGMENTS

This work was supported in part by the Nuclear Criticality Safety Program which is funded and managed by the National Nuclear Security Administration for the US Department of Energy. Additional support for earlier parts of this work came from the Research Council of Norway and the Office of Nuclear Physics of the US Department of Energy.

[1] M. Lugaro, A. M. Davis, R.Gallino, J. J. Pellin, O. Straniero, and F. Kaeppeler, **593**, 486 (2003).
[2] Z. Y. Bao, H. Beer, F. Käppeler, F. Voss, K. Wisshak, and T. Rauscher, Atomic Data and Nucl. Data Tables **75**, 1 (2000).
[3] I. Dillmann, M. Heil, F. Käppeler, R. Plag, T. Rauscher, and F.-K. Thielemann, in *Capture Gamma-Ray Spectroscopy and Related Topics: 12th International Symposium*, edited by A. Woehr and A. Aprahamian (American institute of Physics, Melville, New York, 2006), p. 123.
[4] I. Dillmann, R. Plag, F. Käppeler, and T. Rauscher, in *EFNUDAT Fast Neutrons - Scientific Workshop on Neutron Measurements, Theory, and Applications - Nuclear Data for Sustainable Nuclear Energy*, edited by F.-J. Hambsch (Publication Office of the European Union, Geel, Belgium, 2009), p. 55.
[5] D. J. Hughes and J. A. Harvey, Phys. Rev. **99**, 1032 (1955).
[6] H. S. Camarda, Phys. Rev. C **49**, 1391 (1994).
[7] P. E. Koehler, Phys. Rev. C **84**, 034312 (2011).
[8] P. E. Koehler, F. Bečvář, M. Krtička, J. A. Harvey, and K. H. Guber, Phys. Rev. Lett. **105**, 072502 (2010).
[9] P. E. Koehler, R. Reifarth, J. L. Ullmann, T. A. Bredeweg, J. M. O'Donnell, R. S. Rundberg, D. J. Vieira, and J. M. Wouters, Phys. Rev. Lett. **108**, 142502 (2012).
[10] P. E. Koehler, J. L. Ullmann, T. A. Bredeweg, J. M. O'Donnell, R. Reifarth, R. S. Rundberg, D. J. Vieira, and J. M. Wouters, Phys. Rev. C **76**, 025804 (2007).
[11] P. E. Koehler, Y. M. Gledenov, T. Rauscher, and C. Frōhlich, Phys. Rev. C **69**, 015803 (2004).
[12] P. E. Koehler, A. C. Larsen, M. Guttormsen, S. Siem, and K. H. Guber, Phys. Rev. C **88**, 041305 (2013).

[13] P. Fanto, Y. Alhassid, and H. A. Weidenmuller, Phys. Rev. C **101**, 014607 (2020).
[14] A. C. Larsen, M. Guttormsen, M. Krtička, B. E., A. Burger, A. Gorgen, H. T. Nyhus, J. Rekstad, A. Schiller, S. Siem, et al., Phys. Rev. C **83**, 034315 (2011).
[15] H. Utsunomiya, S. Goriely, T. Kondo, C. Iwamoto, H. Akimune, T. Yamagata, H. Tayokawa, H. Harada, F. Kitatani, Y. W. Lui, et al., **88**, 015805 (2013).
[16] A. Chambers, Tech. Rep., U.S. Department of Energy (2019).
[17] N. Leclaire, I. Duhamel, and M. Monestier, in *Criticality Safety - Pushing Boundaries by Modernizing and Integration Data, Methods, and Regulations*, edited by C. Associates (American Nuclear Society, 2017), p. 15.
[18] D. Brown, M. Chadwick, R. Capote, A. Kahler, A. Trkov, M. Herman, A. Sonzogni, Y. Danon, A. Carlson, M. Dunn, et al., Nuclear Data Sheets **148**, 1 (2018).
[19] C. J. Dean, P. J. Smith, and R. J. Perry, in *International Conference on Nuclear Data for Science and Technology 2007*, edited by O. Bersillon, F. Gunsing, E. Bauge, R. Jacqmin, and S. Leray (EDP Sciences, 2007), p. 829.
[20] S. F. Mughabghab, *Atlas of Neutron Resonances: Resonance Parameters and Thermal Cross Sections Z=1-100* (Elsevier, Amsterdam, The Netherlands, 2006).
[21] S. I. Sukhoruchkin, Z. N. Soroko, and V. V. Deriglazov, *Low Energy Neutron Physics* (Springer-Verlag, Berlin, 1998).
[22] H. Weigmann, G. Rohr, and J. Winter, in *Third Conference on Neutron Cross Sections and Technology*, edited by J. B. Garg (University of Tennessee, Knoxville, 1971), p. 513.
[23] M. Krticka, F. Becvar, I. Tomandl, G. Rusev, U. Agvaanluvsan, and G. E. Mitchell, **77**, 054319 (2008).
[24] A. Emsallem and M. Asghar, **275**, 157 (1975).
[25] A. R. de L. Musgrove, B. J. Allen, J. W. Boldeman, and R. L. Macklin, Nucl. Phys. **A270**, 108 (1976).
[26] R. Bahran, D. Barry, R. Block, G. Leinweber, M. Rapp, A. daskalakis, E. Blain, D. williams, B. McDermott, L. Leal, et al., Phys. Rev. C **92**, 024601 (2015).
[27] J. A. Harvey, D. J. Hughes, R. S. Carter, and V. E. Pilcher, Phys. Rev. **99**, 10 (1955).
[28] H. E. Jackson, **127**, 1687 (1962).
[29] H. Weigmann and H. Schmid, Nucl. Phys. **A104**, 513 (1967).
[30] C. Coceva, F. Corvi, P. Giacobbe, and C. Carraro, Nucl. Phys. **A117**, 586 (1968).
[31] S. Wynchank, J. B. Garg, and W. W. H. andJ. Rainwater, Phys. Rev. **166**, 1234 (1968).
[32] H. Shwe and R. E. Cote, Phys. Rev. **179**, 1148 (1969).
[33] J. Julien, R. Alves, S. de Barros, V. D. Huynh, J. Morgenstern, and C. Samour, Nucl. Phys. **A132**, 129 (1969).
[34] S. A. Sheets, U. Agvaanluvsan, J. A. Becker, F. Bečvář, T. A. Bredeweg, R. C. Haight, M. Krtička, M. Jandel, G. E. Mitchell, J. M. O'Donnell, et al., Phys. Rev. C **76**, 064317 (2007).
[35] T. F. Wang, A. Meaze, M. U. Khandaker, M. S. Rahman, G. N. Kim, L. P. Zhu, H. Xia, Z. Zhou, Y. Oh, H. Kang, et al., Nuclear Instruments and Methods in Physics Research **B266**, 561 (2008).
[36] G. Leinweber, D. P. Barry, J. A. Burke, N. J. Drindak, Y. Danon, R. C. Block, N. C. Francis, and B. E. Moretti, Nuclear Science and Engineering **164**, 287 (2010).
[37] R. M. Bahran, Ph.D. thesis, Rensselaer Polytechnic Institute (2013).
[38] P. E. Koehler, Y. M. Gledenov, J. Andrzejewski, K. H. Guber, S. Raman, and T. Rauscher, Nucl. Phys. **A688**, 86c (2001).
[39] R. W. Peelle, J. A. Harvey, F. C. Maienschein, L. W. Weston, D. K. Olsen, D. C. Larson, and R. L. Macklin, Tech. Rep. ORNL/TM-8225, Oak Ridge National Laboratory (1982).
[40] K. H. Böckhoff, A. D. Carlson, O. A. Wasson, J. A. Harvey, and D. C. Larson, Nucl. Sci. and Eng. **106**, 192 (1990).
[41] K. H. Guber, D. C. Larson, P. E. Koehler, R. R. Spencer, S. Raman, J. A. Harvey, N. W. Hill, T. A. Lewis, and R. R. Winters, in *International Conference on Nuclear Data for Science and Technology*, edited by G. Reffo, A.Ventura, and C. Grandi (Societa Italiana di Fisica, Bologna, 1997), p. 559.
[42] R. L. Macklin, J. Halperin, and R. R. Winters, Nucl. Instrum. and Meth. **164**, 213 (1979).
[43] D. C. Larson, N. M. Larson, J. A. Harvey, F. G. Perey, D. E. Pierce, and R. H. Seals, Tech. Rep. ORNL/TM-9097, Oak Ridge National Laboratory (1985).
[44] N. M. Larson, Tech. Rep. ORNL/TM-9179/R2, Oak Ridge National Laboratory (1989).
[45] P. E. Koehler, R. R. Spencer, R. R. Winters, K. H. Guber, J. A. Harvey, N. W. Hill, and M. S. Smith, Phys. Rev. C **54**, 1463 (1996).
[46] P. E. Koehler, R. R. Winters, K. H. Guber, T. Rauscher, J. A. Harvey, S. Raman, R. R. Spencer, J. C. Blackmon, D. C. Larson, D. W. Bardayan, et al., Phys. Rev. C **62**, 055803 (2000).
[47] W. Rapp, P. E. Koehler, F. Käppeler, and S. Raman, Phys. Rev. C **68**, 015802 (2003).
[48] See Supplemental Material at [URL will be inserted by publisher] for tables of resonance parameters and figures illustrating them and corrections applied to obtain the average resonance parameters, and comparisons to previous work.
[49] T. Fuketa and J. A. Harvey, Nucl. Instrum. Methods **33**, 107 (1965).
[50] C. E. Porter and R. G. Thomas, Phys. Rev. **104**, 483 (1956).
[51] M. Asghar, C. M. Chaffey, M. C. Moxon, N. J. Pattenden, E. R. Rae, and C. A. Uttley, Nucl. Phys. **76**, 196 (1966).
[52] F. H. Fröhner, Tech. Rep. GA-8380, General Atomic, Inc. (1968).
[53] S. P. Kapchigashev and Y. P. Popov, in *Neutron Interactions* (Joint Inst. for Nucl. Res., Dubna No. 1845, Dubna, Russia, 1964), p. 104.
[54] R. R. Winters and R. L. Macklin, Astrophys. J. **313**, 808 (1987).
[55] H. Beer, F. Voss, and R. R. Winters, Astrophys. J. Suppl. **80**, 403 (1992).
[56] L. Koester, K. Knopf, and W. Waschkowski, Z. Phys. A **326**, 227 (1987).
[57] M. I. Pevzner, Y. V. Adamchuck, L. S. Danelyan, B. B. Efimov, S. S. Moskalev, and G. V. Muradyan, Soviet Physics JETP **17**, 803 (1963).
[58] B. J. Allen, J. Boldeman, and R. L. Macklin, Nuclear Science and Engineering **82**, 230 (1982).
[59] B. Allen, J. Gibbons, and R. Macklin, Advances in Nuclear Physics **4**, 205 (1971).

[60] P. E. Koehler, J. A. Harvey, R. R. Winters, K. H. Guber, and R. R. Spencer, **64**, 065802 (2001).

[61] F. Voss, K. Wisshak, K. Guber, F. Käppeler, and G. Reffo, Phys. Rev. C **50**, 2582 (1994).

[62] K. Wisshak, F. Voss, and F. Käppeler, Phys. Rev. C **54**, 2732 (1996).

[63] P. E. Koehler, J. Ullmann, A. Couture, and S. Mosby, in *Compound Nuclear Reactions, CNR*18*, edited by J. Escher, Y. Alhassid, L. A. Berstein, D. Brown, C. Frohlich, P. Talou, and W. Younes (Springer, 2021), p. 187.

[64] T. von Egidy and D. Bucurescu, Phys. Rev. C **80**, 054310 (2009).

[65] A. J. Koning, S. Hilaire, and M. C. Duijvestijn, in *Proceedings of the International Conference on Nuclear Data for Science and Technology - ND2007*, edited by O. Bersillon, F. Gunsing, E. Bauge, R. Jacqmin, and S. Leray (EDP Sciences, Les Ulis, France, 2008), p. 211.

[66] M. Chadwick, P. Obložinský, M. Herman, N. Greene, R. McKnight, D. Smith, P. Young, R. MacFarlane, G. Hale, S. Frankle, et al., Nuclear Data Sheets **107**, 2931 (2006).